Simulation of Air Gap Thickness Variations on Air Spindle Vibrations in Ultra Precision Machine Tools

M. Akhondzadeh*
Mechanical Engineering Department,
Islamic Azad University, Ahvaz branch, Khuzestan, Iran
E-mail: m_akhondzadeh@iauahvaz.ac.ir
*Corresponding author

M. Vahdati
Mechanical Engineering Department,
K. N. Toosi University of Technology, Tehran, Iran
E-mail: Vahdati@kntu.ac.ir

Received: 24 April 2012, Revised: 27 August 2012, Accepted 4 September 2012

Abstract: Air spindles are one of the main elements of precise machine tools. Vibration of these spindles is one of the vital issues necessary for investigation. Among parameters which influence air spindle vibrations are rotational speed, compression air method, input nozzle diameter, air gap pressure. In this study using ANSYS, the effects of air gap thickness on air spindle vibrations have been investigated. In this simulation the air gap is modelled by numbers of linear springs. Then the effect of air gap thickness on air spindle vibrations has been investigated. Rotor externally rotates around stator. Simulation results indicate that for static and transient analysis the values of radial displacements of rotor reduce by decreasing spring length (i.e. rotor and stator gap), and its minimum value are equal to 3.634 μm and 15.6 nm, respectively. Because of constant spring stiffness, in modal and harmonic analysis, results for different spring length have no variation and are equal to 1.053 mm and 23.7 nm, respectively.

Keywords: Air Bearing, Air Spindle, Simulation, Spindle Vibration, Ultra Precision Machine

Reference: Akhondzadeh, M. and Vahdati, M., "Simulation of air pad shape on pressure distribution in air gap of air table in ultra precision machine tools", Int J of Advanced Design and Manufacturing Technology, Vol. 6/ No. 2, 2013, pp. 21-28.

Biographical notes: M. Akhondzadeh received his MSc in mechanical engineering from University of K. N. Toosi University of Technology in 2011. He is currently a faculty member at the department of engineering, IAU Ahwaz branch, Khuzestan, Iran. His current research interest includes Ultra Precision Machining and Nanomachining. **M. Vahdati** is assistant professor of mechanical engineering at the K. N. Toosi University of Technology, Tehran, Iran. He received his PhD and MSc in Manufacturing engineering from Utsunomiya University of Japan. His current research focuses on Ultra Precision Machining, Nanomachining, and Abrasive Fluid Machining.

1 INTRODUCTION

Increasing demand for manufacturing precise components for computers, electronics, nuclear energy and defence applications have caused the advent of ultra precision machining processes. Examples of these components are as optical mirrors, computer memory discs, and drums for photocopying machines, which contain a surface finish of nanometer range and a form accuracy of micron or the sub-micron range. These machines have high precision motion mechanisms. Spindles and tables move on a thin film of compressed air. This air film prevents metals from contact and decreases friction and therefore heat generation, as well as decreasing vibration of the work piece. Thus good surfaces may be achieved.

Pressurized air, before entering into air gap, enters a pad that reduces its instabilities such as turbulence; because it may affect air spindle vibrations. Thus, pressurized air feeding characteristics such as orifice diameter, restriction method, air film thickness, and pressure distribution in air gap, may affect the vibration phenomenon.

Due to the fact that air is a compressible fluid it may be considered to have springiness rate or stiffness. Higher pressures are essentially supposed to be a preload on that air spring. The factors that determine stiffness in air bearings are the pressure in air gap, the thickness of the air gap, and the projected surface area of the bearing [1]. In this study, the effect of air film thickness on air spindle vibrations will be analyzed with simulating it by series of springs in the gap distance between stator and rotor.

Fig. 1 shows mass-spring system for an air bearing. The stator and rotor may be assumed as mass and air springiness has been shown as spring coils. The air pressure distribution in the gap has been assumed constant. This is achievable in practice by using porous type or multiple micro-hole air bearings.

In 2002, Chen et al. [2] from Taiwan, investigated an arc type aerostatic grooved bearing. They studied an aerostatic bearing with four axial and circumferential shallow grooves theoretically. They also analyzed effect of air film thickness, and as well as investigating pressure distribution in grooved and un-grooved bearing. In 2002, Chen and Lin [3] presented a work on static behavior and dynamic stability analysis of grooved rectangular aerostatic thrust bearings, where the studied bearing had X-type grooves. They have analyzed these bearings by theory and experiment and reported same results for air gap thickness.

In 2010, Chen et al. [4] theoretically and experimentally analyzed a compound restrictor circular gas bearing with three straight and arc shallow grooves machined on its surface and reported same results for air film thickness effects. In 2002, Fan and Ho from Taiwan and Mou from Arizona [5] presented an aerostatic air bearing system with multiple micro-holes. They have prototyped multiple micro-holes instead of porous type air bearing. Using porous material or multiple micro-holes will help having constant pressure distribution in air gap.

In 2002, Bang and Lee [6] from South Korea simulated an air spindle by finite element method for analyzing its dynamic behavior. They have used nonlinear springs for air film simulation and have considered two materials aluminium and carbon. They discussed on displacement and run out of spindle center in their work.

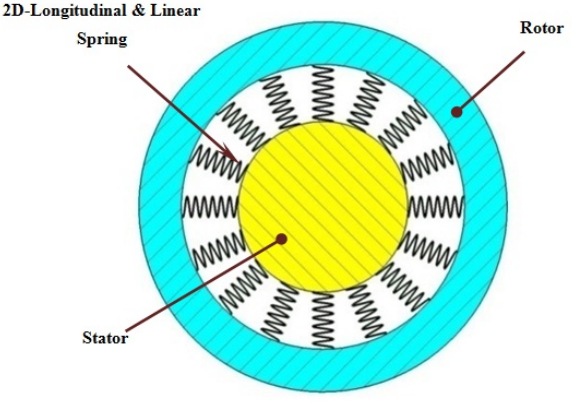

Fig. 1 Schematic mass-spring system equal to air spindle

2 AIR BEARING EQUATIONS

For an aerostatic journal bearing, as shown in Fig. 2(a), air is supplied from an external pressure source and passes through entries with orifice compensation as shown in Fig. 2(b). Orifices are located double-rows about symmetry plane and evenly around the circumference of the bearing.

Assuming the air as perfect gas which is compressible, isothermal and laminar, the non-dimensional Reynolds equation could be derived from Navier–Stokes and continuity equations. In the two dimensional Cartesian coordinates it may be shown as:

$$\frac{\partial}{\partial\theta}\left[\bar{h}^3\frac{\partial\bar{p}^2}{\partial\theta}\right]+\left(\frac{\partial}{L}\right)^2\frac{\partial}{\partial\bar{z}}\left[\bar{h}^3\frac{\partial\bar{p}^2}{\partial\bar{z}}\right]=2\Lambda\frac{\partial}{\partial\theta}\left(\bar{p}\bar{h}\right)+4\gamma\Lambda\frac{\partial\left(\bar{p}\bar{h}\right)}{\partial\tau} \qquad (1)$$

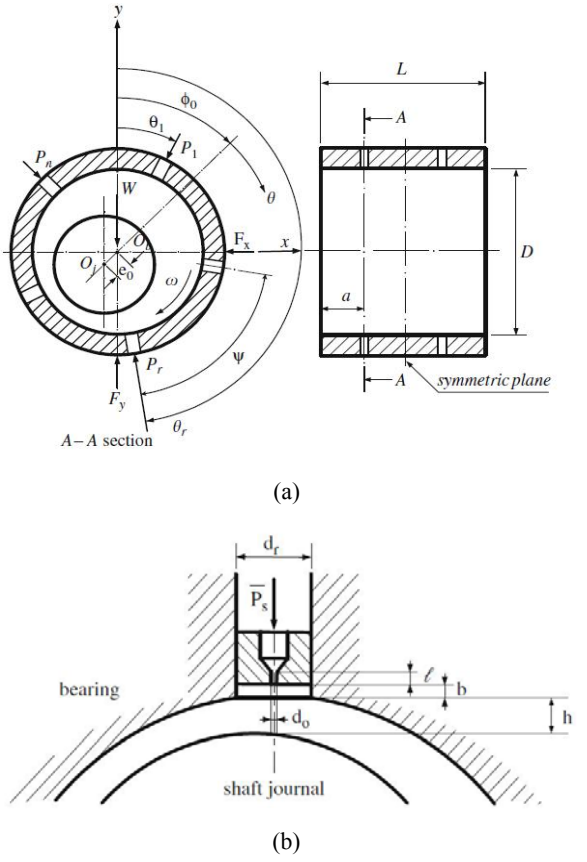

Fig. 2 Configurations of (a) an aerostatic bearing with double-array entries compensated by (b) orifice restriction

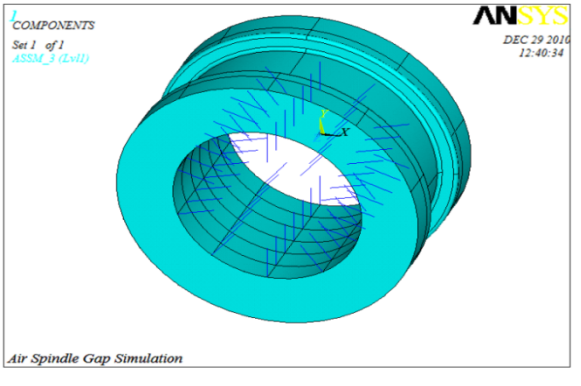

Fig. 3 Modeled rotor and springs in ANSYS software

3 PROCEDURE

In order to investigate effects of air film thickness on spindle vibrations, the static, modal, harmonic and transient analysis were accomplished by ANSYS. Applied elements were SOLID285 for rotor and SPRING14 for springs (air film). For air film simulation, the spring's stiffness considered equal to 30000 N/mm [7]. Also, four values are selected for spring's length that indicates air film thicknesses. Fig. 3 shows modelled rotor with springs in ANSYS.

The rotor material was selected as stainless steel with elasticity module and density equal to 200 GPa and 7860kg/m^3, respectively [6]. Spring's end points are constrained in all degrees of freedom, where meshed rotor is shown in Fig. 4.

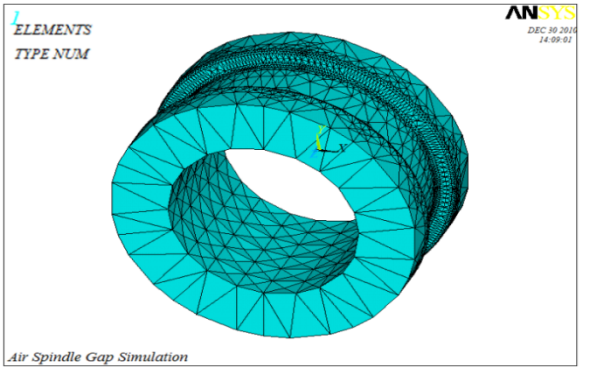

Fig. 4 Meshed rotor in ANSYS software

The air film is simulated by 70 linear springs that every spring has been divided into 1 element. The springs are arranged in 7 rows with equal linear distances and in 10 columns with 36° angular space in circumference. The rotor elements and nodes number equal to 39118 and 8944 respectively.

Fig. 5 shows meshed springs. In order to apply the load on rotor, 5 forces with 10 N on one end edge of rotor has been used. Figs. 6 and 7 show constrains on springs elements and loading on rotor, respectively. In this work, the modal analysis is selected for free vibration, harmonic analysis for forced vibration and transient analysis for time dependent vibration simulations.

4 RESULTS

The results from this simulation can be explored separately i.e. static, modal, harmonic and transient analyses.

4.1. Static Analysis

Maximum displacement and deformation of rotor are the results that concluded from static analysis. Fig. 8 shows the static analysis result for spring lengths equal to 5 mm and 15 mm.

Fig. 8 shows maximum displacement of rotor with 5 mm and 15 mm spring length for static analysis.

Maximum displacements here equals to 3.718 and 8.865 microns, respectively.

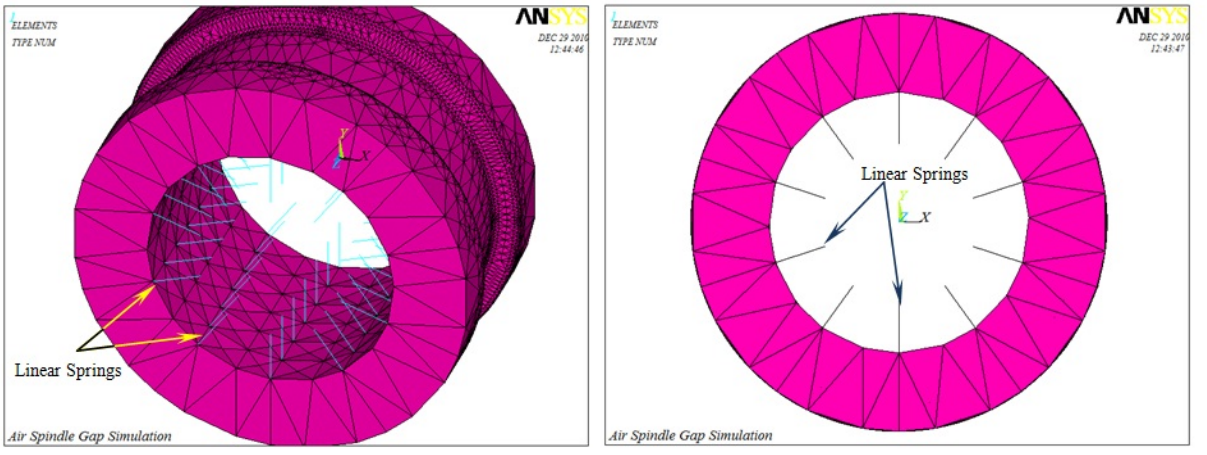

Fig. 5 Meshed springs in inner surface of rotor

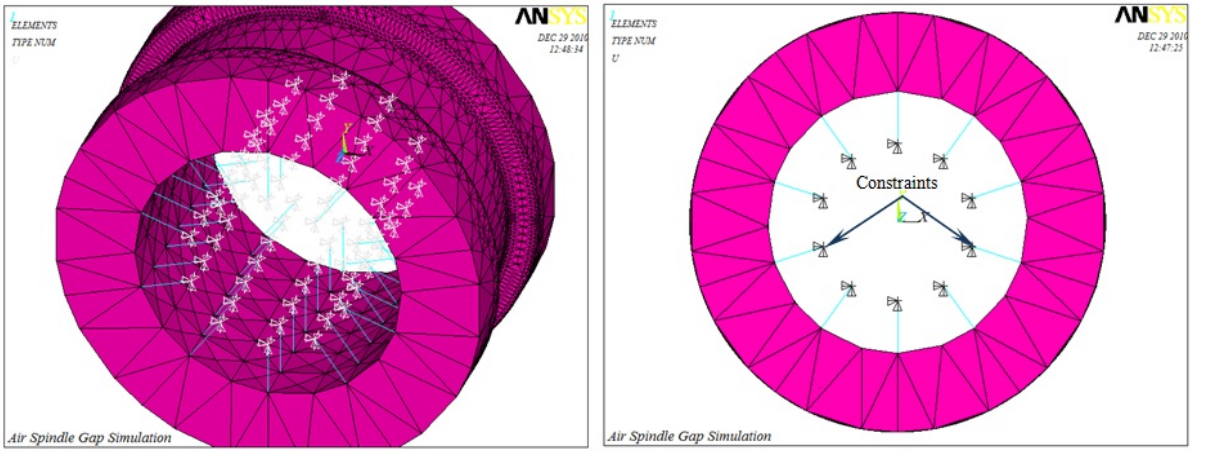

Fig. 6 Constraints on springs end in all DOF

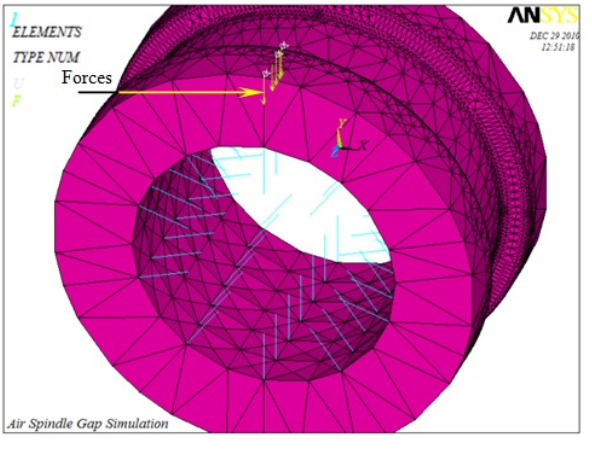

Fig. 7 Loading on rotor with 5 forces

4.2. Model Analysis

For analyzing air spindle free vibrations, Block Lanczos method has been used to vibration modes concluding. Frequency domains considered as 0 to 1500 Hz. Because of the natural frequency dependency on mass and spring stiffness and because these values are constant for rotor, thus natural frequencies for all spring lengths were equal and have listed in Table 1.

Table 1 Natural frequencies derived from air spindle free vibrations simulation

Step	Freq (Hz)
1	0.38E-4
2	174.47
3	174.50

Fig. 9 shows maximum radial displacement of rotor that is equal for all spring lengths, which for resonance frequency is 1.053 mm.

4.3. Harmonic Analysis

The Full Method is employed for air spindle forced vibration analysis. Also, Sparse solver is used too. Harmonic frequency domain is considered as %80 of frequencies from modal analysis. Thus, harmonic frequency domain was considered to be between 0 to 139.6 Hz. Fig. 10 shows rotor radial displacement for 1 mm and 10 mm spring length, where the maximum displacement for all spring length was 23.7 nm.

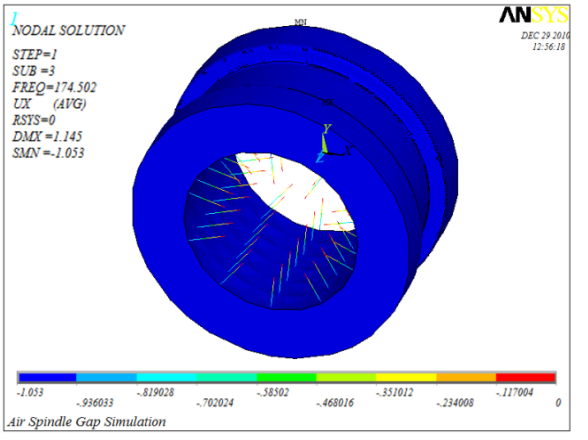

Fig. 9 Modal analysis result in resonance frequency

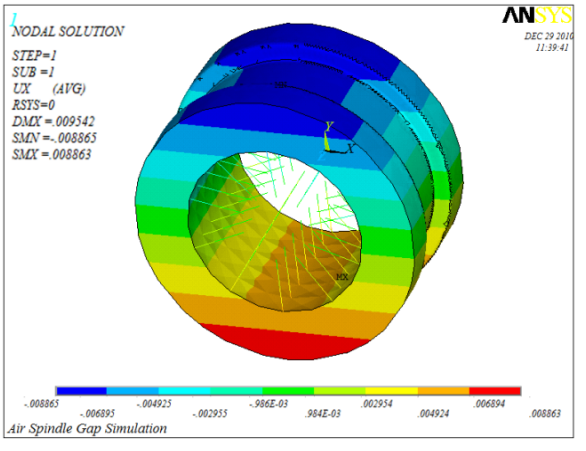

(b) Spring length: 15 mm

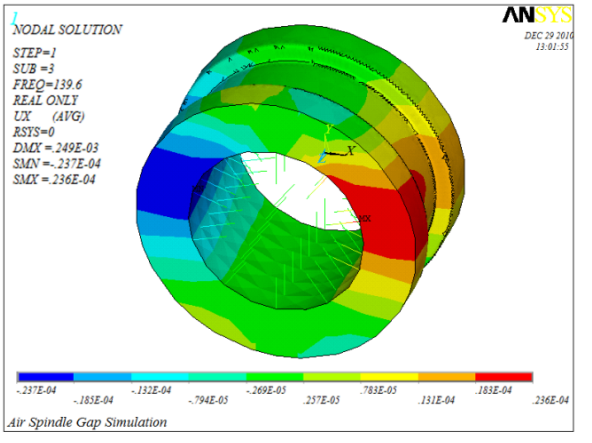

(a) Spring length: 10 mm

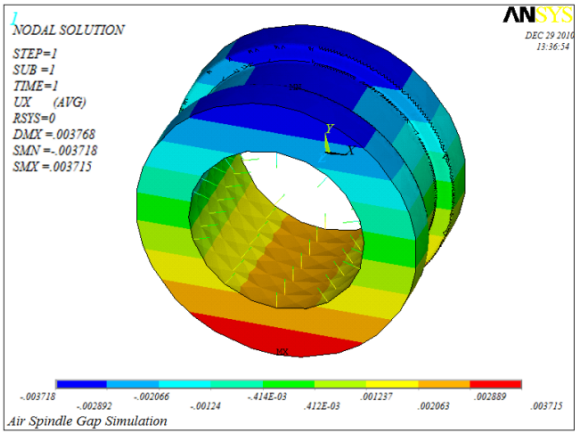

(a) Spring length: 5 mm

Fig. 8 Static analysis result

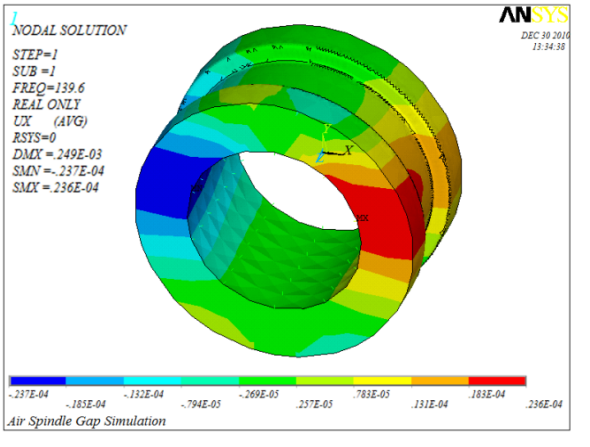

(b) Spring length: 1 mm

Fig. 10 Harmonic analysis result

4.4. Transient Analysis

The Full Method was selected for air spindle time dependent vibrations simulation. Steps for transient analysis were 5 and sub-steps were considered to be 3. Fig. 11 shows displacement versus time values that are listed in Table 2 in radial directions of X and Y. Sprig length is supposed to be 1 mm. This graph is plotted for the same node for spring and internal surface of rotor.

Table 2 Considered Times for transient analysis

Step	Time (Sec)
1	0.1
2	0.821
3	1.641
4	2.462
5	3.283

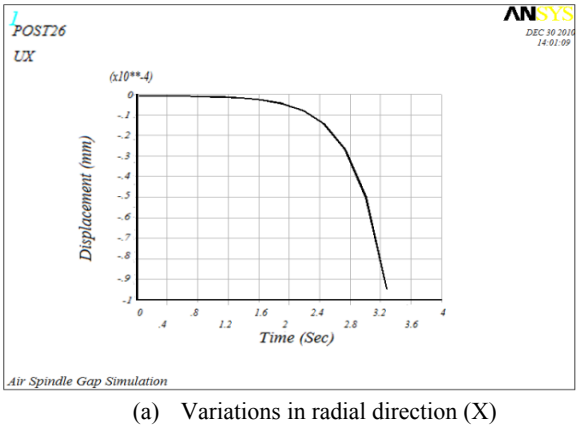

(a) Variations in radial direction (X)

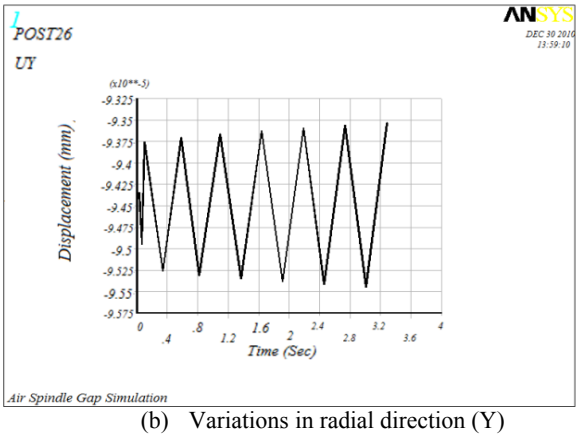

(b) Variations in radial direction (Y)

Fig. 11 Displacement vs. Time from transient analysis (Spring length: 1 mm)

Also, rotor displacement value for 1 mm spring length is shown in Fig. 12 which is equal to 156 nm.

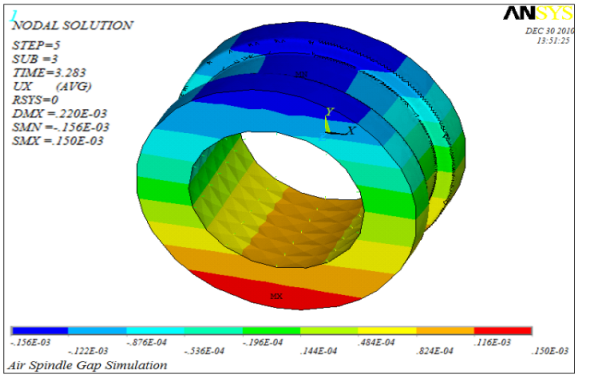

Fig. 12 Time dependent analysis result (Spring length: 1mm)

Simulation results for all analysis are listed in Table 3. Figs. 13 and 14 show displacement vs. spring length for static and transient analysis respectively. Fig. 15 shows the result of [3, 4, and 5] for their theoretical and experimental investigations. From Fig. 15, the bearing load capacity has increased by air film thickness reduction.

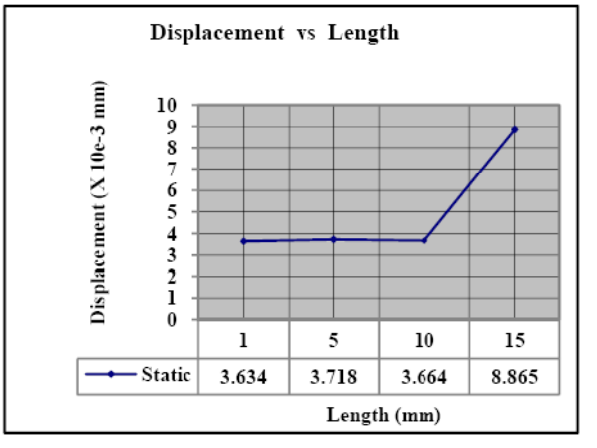

Fig. 13 Displacement vs. spring length plot from static analysis

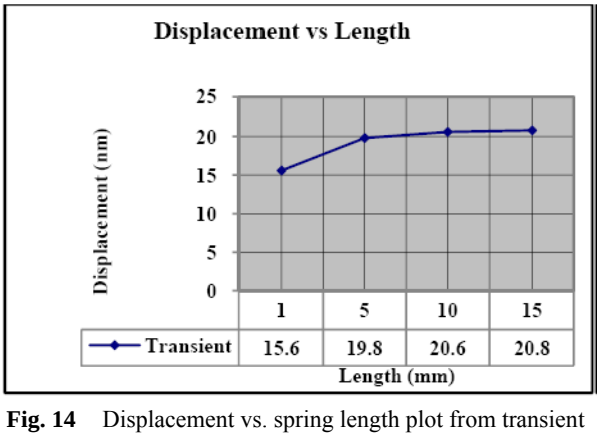

Fig. 14 Displacement vs. spring length plot from transient analysis

Table 3 Maximum displacements from simulation in radial direction

Spring length (mm)	Static analysis (μm)	Modal analysis in resonance frequency (mm)	Harmonic analysis in 80% of resonance frequency (nm)	Transient analysis (nm)
1	3.634	1.053	23.7	15.6
5	3.718			19.8
10	3.664			20.6
15	8.865			20.8

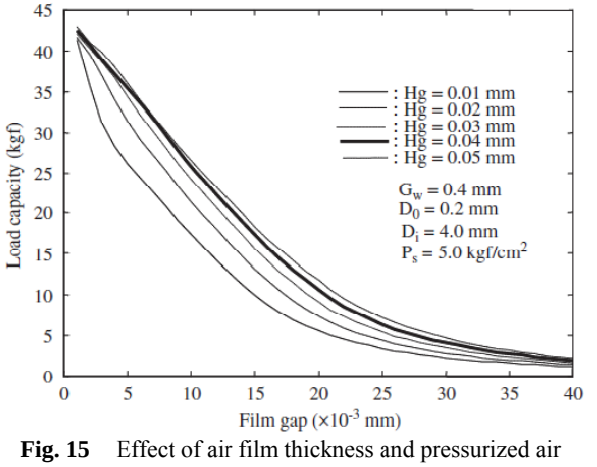

Fig. 15 Effect of air film thickness and pressurized air feeding parameters on load capacity [4]

5 CONCLUSION

1. From static analysis, rotor deformations reduce by springs length reduction. Minimum value equals to 3.634 μm.

2. In modal analysis (free vibrations) because of same rotor mass and springs stiffness, the natural frequency and maximum displacement in resonance are the same for all spring lengths.

3. Harmonic analysis results (forced vibrations) in a frequency of %80 of resonance show that increasing or decreasing springs length have no effect on radial displacements of rotor. Displacement value equals to 23.7 nm in this case.

4. From transient analysis (time dependent vibrations), decreasing of springs length caused to reducing rotor radial displacements where in minimum values reaches 15.6 nm.

6 NOMENCLATURE

a	land width of axial flow (m)
b	pocket depth
C	radial clearance of bearing (m)
D	diameter of bearing (m)
d_o	diameter of orifice (m)
d_r	inlet diameter
e_0	steady-state eccentricity
F_x, F_y	force components (N) due to air film in the x and y directions
h, $\bar{h}$	film thickness (m), $\bar{h}=\frac{h}{c}$
L	axial length of bearing (m)
L	supply orifice length (m)
O_b, O_j	bearing center, spindle or journal center
$\bar{p}$	non-dimensional pressure
P_a	atmospheric pressure (N/m^2)
P_1, P_r, P_n	pressure at the 1st, *r*th and *n*th inlet (N/m^2)
P_s, $\bar{P}_s$	supply pressure (N/m2), $\bar{P}_s = {P_s}/{P_a}$
t	time (sec)
W	load capacity(N)
x, y	Cartesian coordinates of air film
z, $\bar{z}$	axial coordinate of bearing, $\bar{z} = {z}/{(L/D)}$
Λ	bearing number, $\Lambda = {6\mu\omega}/{P_a(C/R)^2}$

Ω	whirl frequency of journal center about the equilibrium axis
ψ	circumferential angle between adjacent restrictions, $\psi = {}^{2\pi}/_{n}$
ϕ_o	steady-state attitude angle
μ	dynamic viscosity of air (Ns/m^2)
θ	angular coordinate, $\theta = {}^{x}/_{R}$
θ_r	circumferential position of the *r*th feeding hole
τ	non-dimensional time, $\tau = \Omega t$
ω	spindle speed (rad/s)
γ	whirl ratio

REFERENCES

[1] www.IBSPE.com, "Air bearing application and design guide", IBS Precision Engineering, 2003.

[2] Chen, M. F., Chen, Y. P., and Lin, C. D., "Research on the arc type aerostatic bearing for a PCB drilling station", Tribology International, Vol. 35, 2002, pp. 235-243.

[3] Chen, M. F., and Lin, Y. T., "Static behavior and dynamic stability analysis of grooved rectangular aerostatic thrust bearings by modified resistance network method", Tribology International, Vol. 35, 2002, pp. 329-338.

[4] Chen, M. F., Huang, W. L., and Chen, Y. P., "Design of the aerostatic linear guideway with a passive disk-spring compensator for PCB drilling machine", Tribology International, Vol. 43, 2010, pp. 395-403.

[5] Kuang-Chao, F., Chi-Chung, H., and Jong-I, M., "Development of a multiple-microhole aerostatic air bearing system", Journal of Micromechanics and Microengineering, Vol. 12, 2002, pp. 636-643.

[6] Bang, K. G., and Lee, D. G., "Thrust bearing design for high-speed composite air spindles", Composite Structures, Vol. 57, 2002, pp. 149-160.

[7] Powell, J. W., "Design of Aerostatic Bearings", The Machinery publishing Co. LTD, 1970.